Optical distinguishability of Mott insulators in the time versus frequency domain

Jacob Masur,* Denys I. Bondar,† and Gerard McCaul‡
Department of Physics and Engineering Physics, Tulane University, New Orleans, Louisiana 70118, USA

(Received 14 February 2022; revised 24 May 2022; accepted 24 June 2022; published 18 July 2022)

High harmonic generation (HHG) promises to provide insight into ultrafast dynamics and has been at the forefront of attosecond physics since its discovery. One class of materials that demonstrates HHG are Mott insulators whose electronic properties are of great interest given their strongly correlated nature. Here, we use the paradigmatic representation of Mott insulators, the half-filled Fermi-Hubbard model, to investigate the potential of using the HHG response to distinguish these materials. We develop a heuristic argument based on the Magnus expansion which predicts that distinguishability of Mott insulators will in most cases diminish as the dimensionless parameter $g \equiv aF_0/\omega_0$ becomes large, a result confirmed by numerical simulation. The notable exception is when comparing to a conducting system, which becomes more distinguishable from in the frequency domain at high g.

DOI: 10.1103/PhysRevA.106.013110

I. INTRODUCTION

One of the principal breakthroughs of the last half-century has been the discovery of nonlinear optics, enabled by the invention of the laser [1,2]. Nonlinear effects are expected to play a crucial role in what has been termed the "second quantum revolution" [3], where quantum effects are exploited to develop new technology. It has already been demonstrated that systems exhibiting a nonlinear optical response possess a number of both useful and surprising properties, such as controllability [4–8], optical indistinguishability [9,10], nonuniqueness [11–14], self-focusing [15], the nonlinear Fano effect [16], and many more [17,18].

Within the plethora of nonlinear effects already discovered [19], one of the most promising is high harmonic generation (HHG). First observed in gases, this phenomenon has also been induced by strong fields in atoms and molecules [20–26], the surfaces of both metal and dielectric solids [27–31], and in bulk crystals [32–41]. The ability to generate light at frequencies many multiples greater than the initial excitation provides a tool for observation and manipulation at the attosecond timescale [42–45]. Given inter- and intraatomic electron motion occurs on precisely this timescale, applications of HHG can provide a route to the study of the electronic structure of materials [40,44,46]. Not only does this offer insight into fundamental phenomena, such as tunneling [47], proper understanding of atomic scale properties has many applications, from mixture characterization [48], to faster task-specific electronics [49], and measurements of chirality [50,51] to novel "valleytronics" [52].

Given that HHG offers a higher-resolution window on electron dynamics, it is natural to ask how it might be used to improve material characterization. In the modern era, this process has moved beyond the determination of simple properties, such as conductivity, and focuses instead on microscopic or even atomic properties. To do so, tools, such as scanning tunneling microscopes [53] and electron diffraction [54] have been employed. These have had great success in certain applications but are far from ubiquitous [40]. Meanwhile, high harmonic responses to optical driving has become a useful tool in electronic analysis [46]. Researchers have successfully applied HHG spectroscopy to probe the electronic structure of specific materials [20–41,45,55], and it has even been shown recently that HHG spectra can indicate a critical point of a quantum phase transition from a spin-density wave to a charge-density wave [56]. Taken together, these results indicate that the high harmonic response of materials may be a powerful future tool in the characterization and analysis of of materials in the solid state.

In such a case, one would ideally employ all information that can be gleaned from a material's optical emission—i.e., the full time-domain response. Whereas there is some prospect of obtaining this in the future [46], at present time-resolved measurement of subfemtosecond processes is difficult in the solid state [49,57]. Nevertheless, frequency-domain spectroscopy of high-order harmonics and their relative intensities can be acquired experimentally at the cost of losing the phase information of the response. This begs the question as to the importance of this lost phase information.

Here, we consider the potential of high harmonic optical responses as a tool for material identification whereas placing particular emphasis on the role of the optical response's phase information in distinguishing the driven dynamics of different materials. We investigate this question in a class of materials described by the Hubbard model, namely, Mott insulators [58,59]. Previous studies of HHG in the Hubbard model have revealed that the mechanism for generation of high harmonics is intrinsically distinct from that of crystals and other solids in which HHG has been observed [60,61].

*jmasur@tulane.edu
†dbondar@tulane.edu
‡gmccaul@tulane.edu

Specifically, the plateaus in the optical spectra depend heavily on the dynamics of the charge carriers, doublons, and holes [60], suggesting that the HHG spectra of Mott insulators contain valuable electronic information [62]. This can be illustrated with the consideration that in the regime of linear response, a monchromatic source will generate a relatively narrow emission spectrum which can be difficult to distinguish from the spectra produced by similar materials [10]. The advantage of HHG is that it generates an broad spectrum of response from a monochromatic source, which carries more information about the irradiated material than can be obtained from a single pulse in the linear-response regime. This naturally begs the question as to whether a specific Mott insulator can be characterized and distinguished from others purely by its high harmonic response. This would, in turn, facilitate the parametrization of new materials purely by a spectral measurement.

The rest of this paper will be structured as follows. In Sec. II we set out the the driven Hubbard model and define figures of merit which quantify the relative distinguishability of two systems based on their time or frequency domain response. We also provide a heuristic analysis predicting how the degree of distinguishability of two materials depends on both intrinsic system and laser pulse parameters. Section III presents the results of numerical analysis, identifying the regime in which phase information plays an important role in material characterization. Finally, we close with a discussion of the results and their potential applications in Sec. IV.

II. MODEL

We would like to analyze the responses of different materials to an incident laser pulse which couples electrons to an electric field. Using atomic units ($\hbar = e = 1$), henceforth, unless explicitly stated otherwise, we take the paradigmatic Hubbard model [8,59–62],

$$\hat{H}(t) = -t_0 \sum_{j,\sigma} (e^{-i\Phi(t)} \hat{c}^\dagger_{j,\sigma} \hat{c}_{j+1,\sigma} + \text{H.c.}) + U \sum_j \hat{n}_{j,\uparrow} \hat{n}_{j,\downarrow}, \tag{1}$$

where $\hat{c}^\dagger_{j,\sigma}$ and $\hat{c}_{j,\sigma}$ are, respectively, the canonical fermionic creation and annihilation operators at site j with spin σ, $\hat{n}_{j,\sigma} = \hat{c}^\dagger_{j,\sigma} \hat{c}_{j,\sigma}$ is the particle number operator, t_0 is the hopping parameter, U is the on-site interaction parameter, and $\Phi(t) = aA(t)$ is the Peierls phase. This, in turn, is composed of both lattice spacing a and the vector potential $A(t)$, which is related to the electric field by $E(t) = -\partial_t A(t)$.

Although the Hubbard model is a relatively simple description of Mott insulators, it provides rich insight into the strong electron-electron interactions in these materials [58,59,62,63], distinguishing itself from models relying on mean-field approximations. These interactions play a crucial role in the band structure of Mott insulators [60], preventing current flow in these materials with half-filled valence bands that are predicted to be conductors under band theory.

The optical response of the material to driving is quantified by the current operator,

$$\hat{J}(t) = -iat_0 \sum_{j,\sigma} e^{-i\Phi(t)} \hat{c}^\dagger_{j,\sigma} \hat{c}_{j+1,\sigma} - \text{H.c.}, \tag{2}$$

which can be derived from a continuity equation for electron density [8]. The expectation of the current density operator over the course of the evolution gives access to all spatial and temporal information regarding a given material's optical response as the radiated emission will be proportional to $\partial_t J(t)$. Ordinarily, it is easier to measure the spectra rather than the time-resolved HHG output. The spectrum is given by

$$S(\omega) = |\mathcal{F}_{t\to\omega} \partial_t J(t)|^2, \tag{3}$$

where $\mathcal{F}$ denotes the Fourier transform and $J(t) = \langle \hat{J}(t) \rangle$ is the current expectation.

Clearly, the spectrum does not contain any of the phase information present in the corresponding current expectation. We seek to determine not only the degree to which one is able to distinguish between systems via their optical response, but whether phase information materially affects this distinguishability. In order to assess the relative distinguishability of two systems (indexed by i and j), we define two relative distance functions for a set of current expectations and their spectra,

$$\mathcal{D}_t(i,j) = \mathcal{N}_t \sqrt{\int_0^T \left(\frac{\partial_t J_i(t)}{n_i^t} - \frac{\partial_t J_j(t)}{n_j^t} \right)^2 dt}, \tag{4}$$

$$\mathcal{D}_p(i,j) = \mathcal{N}_p \sqrt{\int_0^{\omega_c} \left(\log_{10} \frac{S_i(\omega)}{n_i^\omega} - \log_{10} \frac{S_j(\omega)}{n_j^\omega} \right)^2 d\omega}, \tag{5}$$

$$n_i^t = \max_{t\in[0,T]} \partial_t J_i(t), \quad n_i^\omega = \max_{\omega\in[0,\omega_c]} S_i(\omega), \tag{6}$$

$$\mathcal{N}_t = \frac{1}{\max_{i,j} \tilde{\mathcal{D}}_t(i,j)}, \quad \mathcal{N}_p = \frac{1}{\max_{i,j} \tilde{\mathcal{D}}_p(i,j)}. \tag{7}$$

Here, $\mathcal{D}_t(i,j)$ denotes the distance in the time domain, $\tilde{\mathcal{D}}_t(i,j)$ is the unnormalized distance in the time domain, $\mathcal{D}_p(i,j)$ denotes the distance in the frequency domain, and $\tilde{\mathcal{D}}_p(i,j)$ is the unnormalized distance in the time domain. Each distance measure is normalized to the maximum value over the set of pairs, giving a *relative* distinguishability that allows the otherwise incommensurate distance measures of the two domains to be compared directly. T is the duration of the pulse, and ω_c is the cutoff frequency defined as the minimum frequency for which $S_i(\omega_c) = 10^{-20}$ or $S_j(\omega_c) = 10^{-20}$, choosing whichever ω_c is smaller. Note that each scaled by its maximum value over the pulse $n_i^{t/\omega}$, reflecting the fact that Hubbard dynamics are controlled by the ratio U/t_0 [59], rather than any absolute scaling of the Hamiltonian. This ensures that the distinguishability measures capture genuine differences in the optical dynamics, rather than simple scale variations. Naturally, a distance of zero between two systems indicates identical responses and perfect indistinguishability, whereas a longer distance indicates a higher degree of relative distinguishability.

In equilibrium ($\Phi(t) = 0$) only the ratio of two parameters, the interaction energy U and the hopping energy t_0, determine the electronic properties of a material described by Eq. (1). Consequently, one may scale all parameters to units of t_0, and remove it from consideration. Under driving, however, the dynamics of the optical response depends not only on U/t_0, but also on the lattice constant a and the driving pulse.

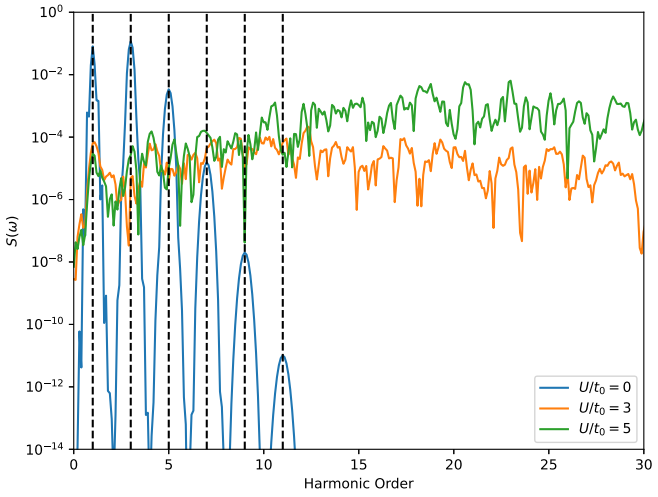

FIG. 1. Power spectra of a conductor ($U/t_0 = 0$) and two Mott insulators ($U/t_0 = 3$ and $U/t_0 = 5$) at $a = 4$ Å and $F_0 = 10\ \frac{\text{MV}}{\text{cm}}$. The vertical lines indicate odd integer harmonics on which the power spectra of the conductor demonstrates well-defined peaks. The upper line of the insulators' spectra is the power spectrum of the $U/t_0 = 3$ system, and the lower one is the spectrum of the $U/t_0 = 5$ system.

For concreteness, we consider driving each system from its ground state with the phase resulting from a transform-limited laser pulse,

$$\Phi(t) = g\,\sin^2\left(\frac{\omega_0 t}{2M}\right)\sin(\omega_0 t), \tag{8}$$

where $M = 10$ is the number of cycles and the dimensionless ratio $g = aF_0/\omega_0$ relates the lattice constant, field strength F_0, and driving frequency ω_0, which we hold constant at 32.9 THz ($\hbar\omega_0/t_0 = 4.2 \times 10^{-2}$) throughout the paper. It is interesting to note the similarity between g and the Hubbard model Keldysh crossover parameter $\gamma = \omega_0/(\xi F_0)$ [64,65], where ξ is the correlation length [66]. This parameter indicates the mechanism for pair production: $\gamma \ll 1$ corresponds to the quantum tunneling regime whereas $\gamma \gg 1$ indicates a multiphoton absorption regime [64].

The response of a given material to optical stimulation depends heavily on the values of U and g that define the material's electronic properties. For Mott insulators, charge is carried by doublon-hole excitations [60], the pair production of which decreases exponentially with U [64]. Figure 1 shows some of the essential optical characteristics resulting from this, such as a white-light response to optical driving in sufficiently strong Mott insulators. In the $U = 0$ conducting limit, the spectral behavior becomes identical to atomic systems [67] with well-defined peaks present at odd harmonics.

There is no simple method for determining the effect of g on material response as the parameter is a combination of both an intrinsic material property (the lattice constant a) and the frequency and amplitude of the driving field. Naturally, this means that it is difficult to disentangle the effect of varying g as being the consequence of either the system or driving field parameters. In the first instance, however, the principal response of a material depends on its intrinsic properties rather than the field driving it (i.e., a conductor vs an insulator). We might, therefore, be able to obtain a heuristic understanding of the zeroth-order effect of scaling g by considering its effect in terms of the intrinsic parameters defining a given system. That is, we can estimate what consequence varying the field parameters (or, equivalently, the system lattice spacing) will have on the effective parametrization of the system without directly considering the full dynamics of the response. To do so, we borrow a commonly used technique from Floquet engineering [68], the Magnus expansion [69]. Using this, it is possible to estimate how in the large g limit this factor affects optical spectra.

Taking $|\psi(t)\rangle = \hat{U}(t)|\psi(0)\rangle$, the system propagator will be of the form

$$\hat{U}(t) = e^{\Omega(t)}. \tag{9}$$

We would like to approximate an effective time-independent Hamiltonian, such that

$$\Omega(t) \approx -i\hat{H}_{\text{eff}}t. \tag{10}$$

The exponent $\Omega(t)$ can itself be expressed in terms of the Magnus expansion,

$$\Omega(t) = \sum_{k=1}^{\infty}\Omega_k(t). \tag{11}$$

The first term in this expansion is given by

$$\Omega_1(t) = -i\int_0^t \hat{H}(t_1)dt_1, \tag{12}$$

with the integral over the two-body term of Eq. (1) being trivial given that it is time independent. Note that it is the higher-order terms of this expansion that are precisely those that will actually generate the high harmonics, but as mentioned previously the first-order term allows one to estimate how (for example) a material may display more metallic or insulator, such as behavior as the field it is subjected to is varied, by approximating its effect on the t_0 and U parameters. Thus, we focus our attention on the integral over the hopping term,

$$\int_0^T dt \sum_{j,\sigma} e^{-i\Phi(t)}\hat{c}^{\dagger}_{j,\sigma}\hat{c}_{j+1,\sigma} + \text{H.c.} \tag{13}$$

$$= \sum_{j,\sigma}\hat{c}^{\dagger}_{j,\sigma}\hat{c}_{j+1,\sigma}\int_0^T dt\, e^{-i\Phi(t)} + \text{H.c.}, \tag{14}$$

where integrating over the duration of the single pulse $T = 2\pi M/\omega_0$. The relevant integral is, therefore,

$$I = \int_0^T dt\ \exp[-igf(t)], \tag{15}$$

where $f(t) = \sin^2(\omega_0 t/2M)\sin(\omega_0 t)$ (see Fig. 2).

Given the envelope is slowly varying relative to ω_0, for each half period π/ω_0, we approximate it by its averaged value over that period,

$$\Delta_j = \frac{1}{2}\left[\sin^2\left(\frac{j\pi}{2M}\right) + \sin^2\left(\frac{(j+1)\pi}{2M}\right)\right]. \tag{16}$$

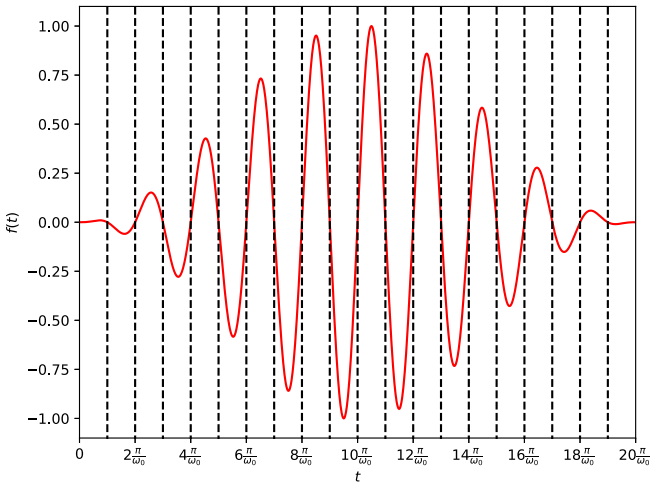

FIG. 2. A plot of $f(t)$ where each dashed line is the boundary of a Δ_j.

Consequently, the integral can be approximated as

$$I \approx \frac{2}{\omega_0}\sum_{j=0}^{M-1}\int_0^{\pi} dt\ \cos[g\Delta_j \sin(t)]$$
$$= \frac{2}{\omega_0}\sum_{j=0}^{M-1} J_0(g\Delta_j), \tag{17}$$

where $J_0(x)$ is the zero-order Bessel function [70, Eq. (10.9.1)]. In the limit of large g, this function may be replaced by its asymptote [70, Eq. (10.17.3)] to obtain

$$I \approx T\sqrt{\frac{1}{g}}\zeta, \tag{18}$$

where

$$\zeta = \frac{2}{T}\sqrt{\frac{2}{\pi}}\sum_{j=0}^{M-1}\frac{1}{\sqrt{\Delta_j}}\cos\left(g\Delta_j - \frac{\pi}{4}\right). \tag{19}$$

Having approximated the integral, it is now possible to state the form of the effective Hamiltonian in Eq. (10),

$$\hat{H}_{\text{eff}} \approx -\frac{\zeta t_0}{\sqrt{g}}\sum_{j,\sigma}(\hat{c}^{\dagger}_{j,\sigma}\hat{c}_{j+1,\sigma} + \text{H.c.}) + U\sum_j \hat{n}_{j,\uparrow}\hat{n}_{j,\downarrow}. \tag{20}$$

This effective Hamiltonian is in the form of the Hubbard Hamiltonian in equilibrium with one important difference, the scaling of the hopping energy by $\zeta/\sqrt{g}$. Note that whereas this effective Hamiltonian will not capture the full dynamics of the system, it does make a concrete prediction on the effective strength of the system's kinetic term in the large g limit.

Note that whereas ζ has some g dependence, this occurs only in the trigonometric terms in the sum, meaning that this parameter will be bounded with respect to g, and have little impact once the response is normalized. This is borne out by numerical calculation of Eq. (15) as shown in Fig. 3. Here it is

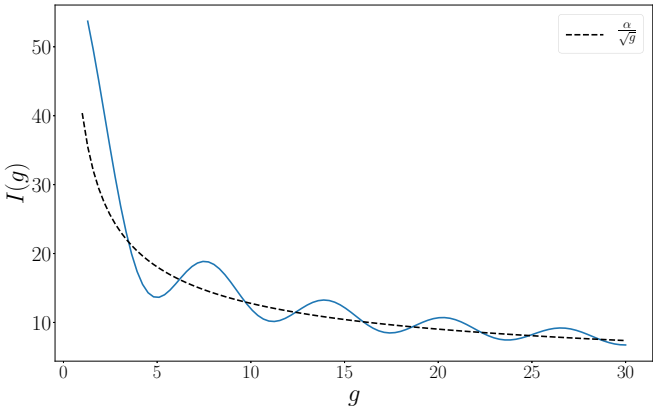

FIG. 3. Numerical calculation of Eq. (15). As expected, the behavior at large g is well described by $\frac{\alpha}{\sqrt{g}}$, where α is some constant of proportionality. The trigonometric dependence of ζ on g introduces small oscillations around the central asymptote.

apparent that the contribution of ζ at large g is the introduction of small oscillations around $\frac{1}{\sqrt{g}}$. It, therefore, follows that the principal effect of increasing g will be the scaling of the system response in the following manner:

$$t_0 \to \frac{t_0}{\sqrt{g}} \quad \Longrightarrow \quad \frac{U}{t_0} \to \frac{U\sqrt{g}}{t_0}. \tag{21}$$

Clearly, for any insulator, the effective ratio of the interaction parameter to the hopping parameter is proportional to the scaling parameter $\sqrt{g}$. This means an increase in g leads to a higher effective ratio. Depending on the value of U, this can potentially transition the system from a regime where hopping dominates to one where the on-site potential dominates the dynamics of the system. This suggests increasing g will trend push all systems towards the high U, strongly insulating regime. The exception to this is the $U = 0$ conducting system, which will only experience a scaling in the magnitude of its optical response, rather than its dynamical character. The same will be true (albeit to a lesser extent) when U is sufficiently small that even after scaling the the parameter ratio is < 1, and the system remains a kinetic-dominated regime.

Thus, when g is increased, we expect that the distance between the responses of two Mott insulators given by Eqs. (4) and (5) to reduce, with the exception of those systems with sufficiently small U that the scaling does not invert the balance between kinetic and potential terms. This is exactly the phenomena illustrated in Fig. 4: At low scaling the two systems have highly distinguishable responses, but at high scaling their power spectra are more similar. The only type of material that will be distinguishable from Mott insulators in the high-g regime are conductors whose response is unaffected by the scaling in Eq. (21).

III. RESULTS

In this section, we numerically investigate the extent to which the degree of distinguishability between systems depends on system U/t_0, a, and pulse parameters F_0 and ω_0. In particular, we demonstrate that there is a comparatively high experimental optical discriminability between many Mott

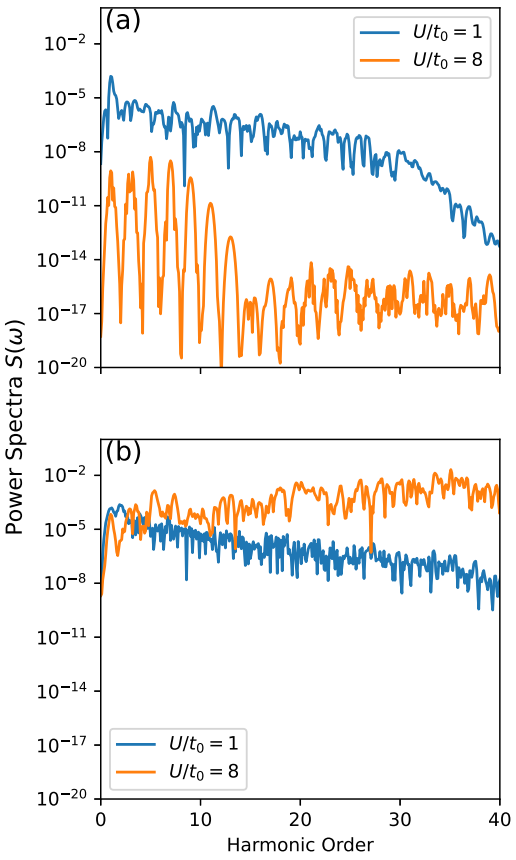

FIG. 4. Spectra of two systems defined by their intrinsic electronic properties ($U/t_0 = 1$ and $U/t_0 = 8$) at two levels of scaling: the spectra in plot (a) are scaled by $g = 4.62$ and the spectra in plot (b) are scaled by $g = 46.2$. In plot (a), the upper line represents the $U/t_0 = 1$ system and the lower line represents the $U/t_0 = 8$ system, and in plot (b), the lower line corresponds to the $U/t_0 = 1$ system whereas the lower line corresponds to the $U/t_0 = 8$ system.

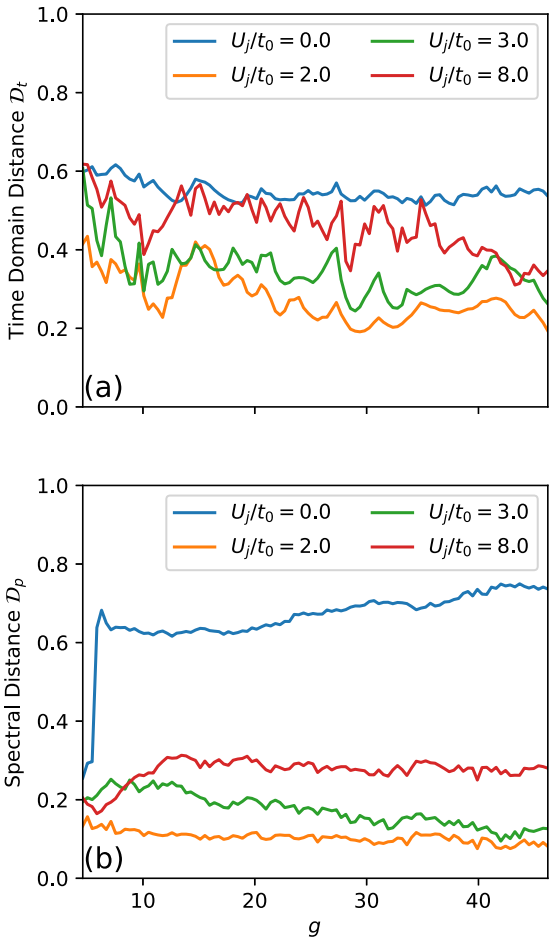

FIG. 5. The distance in the (a) time domain and the (b) frequency domain of comparing $U_i = 1t_0$ to U_j specified by the legend. In both plots, the curves, from top to bottom, correspond to $U_j/t_0 = 0$, 8, 3, and 2.

insulators at a low lattice spacing and low-field strength relative to the driving frequency. Conversely, as predicted in Sec. II, as one increases the factor g, all systems (except near conductors) exhibit behavior associated with the large U/t_0 regime and, hence, become less distinguishable. The increased distinguishability of conductors in this parameter range is also demonstrated.

Pairs of systems distinguished by potentials U_i and U_j are simulated via exact diagonalization in QUSPIN, and evolved using an eighth-order Runge-Kutta method [71]. Current expectations are calculated by constructing the time-dependent operator in (2) at each time step, and taking the expectation value using the state at the corresponding time. From this, the distance measures of Eqs. (4) and (5) are calculated. These distances are then scaled to their maximum value over the total range of parameter pairs considered to give a measure of relative distinguishability. Figure 5 demonstrates the dependence relative distinguishability of several system pairs with respect to g, whereas Fig. 6 reports the relative distinguishability in the time and spectral domains via both the difference ΔU and the average $\bar{U}$ of each system's potential.

The first point to note is that in almost all cases, the relative distinguishability of two systems is greater in the time domain than the spectral domain (i.e., points lie below the diagonal), demonstrating the importance of phase information for distinguishing between system responses. As might be expected, distinguishability tends to be lowest for materials with small ΔU and high $\bar{U}$. The relative distinguishability between the two domains also changes dramatically as g is increased. Taking $U = t_0$ as a reference system, Fig. 5 shows clearly that in the time domain, the distinguishability of the $U = t_0$ system from other insulating systems trends downwards, whereas distinguishability from the conductor remains relatively constant. Interestingly, the distinguishability of the nonconducting systems all appear to share some oscillatory features, consistent with the oscillatory character of the integral shown in Fig. 3. In the spectral domain, the increase in distinguishability relative to a conductor can be seen clearly. This is to be expected, given the scaling argument in Eq. (21). At intermediate g the distinguishability relative to the deeply insulating $U = 8t_0$ increases slightly before plateauing, and this is likely due to the scaling producing a more extreme shift in both the location and magnitude of the $U = 8t_0$ system's spectral peak (as can be seen in Fig. 4).

When examining the distinguishability as a function of both the difference and average U for system pairs, the same

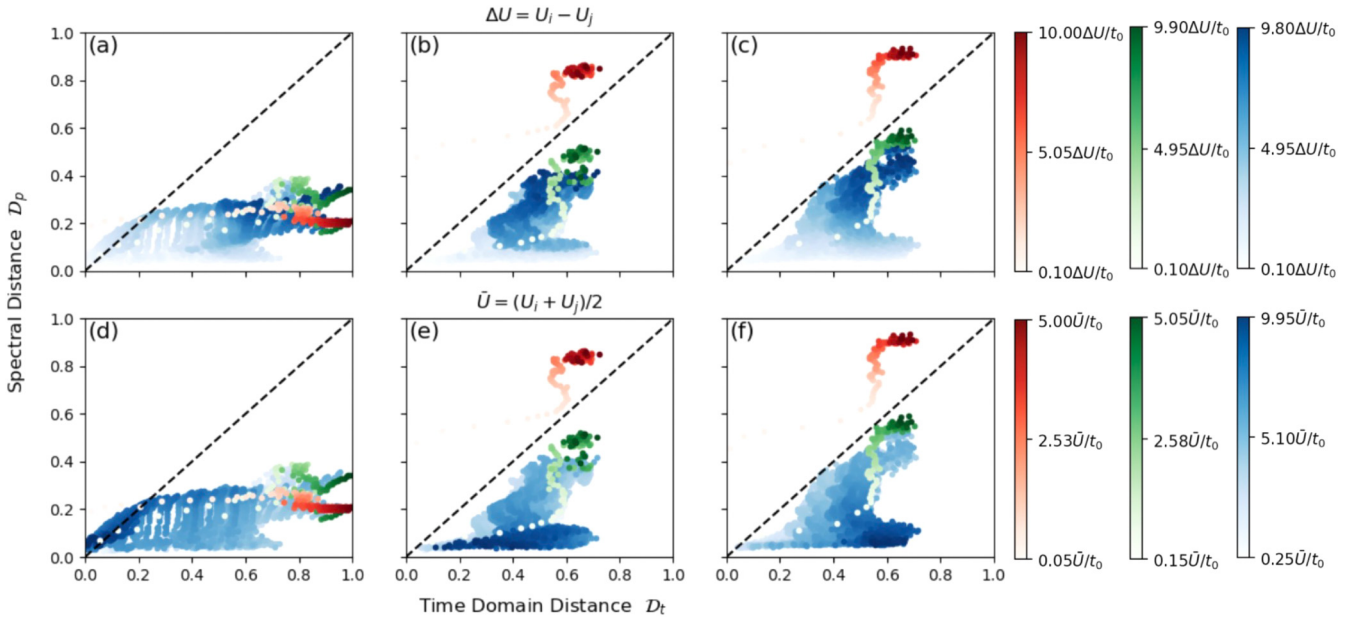

FIG. 6. Each point is a comparisons of two systems with different electronic properties ($U_i \neq U_j$) at the same scaling factor g. Distances in time and spectral domains are scaled by the maximum distance observed in the respective domain over $g \in [4.62, 46.2]$ and $U \in [0, 10t_0]$, so the distance plotted here is unitless in both domains. Systems represented in plots (a) and (d) are driven with $g = 4.62$, those in plots (b) and (e) are driven with $g = 14.7$, and those in plots (c) and (f) are driven with $g = 25.2$. The coloring of the points in plots (a)–(c) and (d)–(f) represents $\Delta U = U_i - U_j$ and $\bar{U} = (U_i + U_j)/2$, respectively, of the systems being compared. A more-saturated color indicates a larger difference or average of the U values, and a less-saturated color indicates a smaller difference or average. The different coloring schemes highlight special comparisons. Red points in all plots are comparisons where one system is a conductor ($U_i = 0$), green points are comparisons to the smallest nonzero value of U_i, $U_1 = 0.1t_0$, and the blue points are all remaining comparisons, that is, comparisons of only insulators.

trend of systems close to the conducting limit increasing in spectral distinguishability with g can be seen in Fig. 6. Since the effective ratio of conductors cannot be scaled by the field strength or lattice constant, conductor response to optical driving cannot be dynamically altered by varying g. A system close to this $U = 0$ limit will still retain its conductorlike properties, whereas a system that is already deeply in the insulating regime is scaled into an even more strongly insulating system. This behavior is most strikingly observed in Fig. 6(c), where at high g a banding effect is observed separating distinguishabilities into those systems where one of the material pair is either a conductor or small U material.

Finally, we find in all cases that whereas increasing g may for some systems increase spectral distinguishability, all pairs in the time domain experience a steady compression of distinguishability as one might expect from Eq. (21). Nevertheless, with the exception of comparisons where one system is conducting, all systems are relatively more distinguishable in the time domain, despite the reduction in distinguishability that occurs at high g [i.e., Figs. 6(c) and 6(f)].

IV. DISCUSSION

Here we have examined the feasibility of distinguishing driven Mott insulators via their optical response. Simulation demonstrated that the importance of phase information in this process was dependent on the applied field strength and confirmed the heuristic argument that the distinguishability of insulators should decrease in the large-g limit. To paraphrase Tolstoy [72], conductors—like happy families—always retain a high degree of distinguishability in one domain or another, whereas the distinguishability of insulating pairs depends strongly on the combination of driving field amplitude, frequency, and system lattice spacing.

The high dependence of material response on the scaling factor g begs the question, what scaling values are physically realizable for high-frequency pulses? Considering a simple subclass of Mott insulators, transition-metal oxides, we determine that 4 Å is a physically realistic lattice constant based on studies performed by Heine and Mattheiss [73]. Hohenleutner *et al.* [36] also experimentally demonstrated pulse generation with a peak field of 44 $\frac{\text{MV}}{\text{cm}}$. Thus, given an infrared frequency 32.9 THz, the scaling factors studied here are certainly within the range of allowed experimental values since these estimates place a maximum scaling at $g = 81.3$. Moreover, the results presented here demonstrate that the change in distinguishability sweeping over a range of field strengths may also serve as a useful source of information for identifying materials.

It is rather interesting to note that the strong dependence of distinguishability on g implies that the Keldysh parameter γ may *also* serve as a proxy for optical distinguishability for systems. Indeed, given this parameter will depend on each system's correlation length (and, therefore, U), it encapsulates more information about each system individually than g alone. A potential future avenue of investigation would there be to study whether a pairwise function of each system's γ may offer some predictive heuristic for their relative distinguishability.

Of particular importance is the finding that experimental differentiation between different Mott insulators is in most cases more easily achieved in the time domain. Whereas spectral characteristics are unquestionably easier to obtain experimentally, the results presented show that the technique of terahertz time-domain spectroscopy [74,75] could profitably be employed to better distinguish between materials.

Although our results only apply to strongly correlated materials, sufficient experimental optical similarity between a known Mott insulator whose atoms are spaced sufficiently and a material with comparable interatomic spacing could provide an aid to the nontrivial problem of distinguishing between a band insulator and a Mott insulator [53].

ACKNOWLEDGMENTS

This work has been generously supported by Army Research Office (ARO) (Grant No. W911NF-19-1-0377; program manager Dr. J. Joseph). J.M. was supported by the ARO Undergraduate Research Apprenticeship Program and the Tulane Honors Summer Research Program. The views and conclusions contained in this paper are those of the authors and should not be interpreted as representing the official policies, either expressed or implied, of the ARO or the U.S. Government. The U.S. Government is authorized to reproduce and distribute reprints for Government purposes notwithstanding any copyright notation herein.

[1] P. A. Franken, A. E. Hill, C. W. Peters, and G. Weinreich, Generation of Optical Harmonics, Phys. Rev. Lett. **7**, 118 (1961).

[2] W. Kaiser and C. G. B. Garrett, Two-Photon Excitation in CaF_2: Eu^{2+}, Phys. Rev. Lett. **7**, 229 (1961).

[3] J. P. Dowling and G. J. Milburn, Quantum technology: the second quantum revolution, Philos. Trans. R. Soc. London, Ser. A **361**, 1655 (2003).

[4] A. Rothman, T.-S. Ho, and H. Rabitz, Observable-preserving control of quantum dynamics over a family of related systems, Phys. Rev. A **72**, 023416 (2005).

[5] A. Magann, T.-S. Ho, and H. Rabitz, Singularity-free quantum tracking control of molecular rotor orientation, Phys. Rev. A **98**, 043429 (2018).

[6] A. G. Campos, D. I. Bondar, R. Cabrera, and H. A. Rabitz, How to Make Distinct Dynamical Systems Appear Spectrally Identical, Phys. Rev. Lett. **118**, 083201 (2017).

[7] G. McCaul, C. Orthodoxou, K. Jacobs, G. H. Booth, and D. I. Bondar, Driven Imposters: Controlling Expectations in Many-Body Systems, Phys. Rev. Lett. **124**, 183201 (2020).

[8] G. McCaul, C. Orthodoxou, K. Jacobs, G. H. Booth, and D. I. Bondar, Controlling arbitrary observables in correlated many-body systems, Phys. Rev. A **101**, 053408 (2020).

[9] B. Busson and A. Tadjeddine, Non-uniqueness of parameters extracted from resonant second-order nonlinear optical spectroscopies, J. Phys. Chem. C **113**, 21895 (2009).

[10] G. McCaul, A. F. King, and D. I. Bondar, Optical Indistinguishability via Twinning Fields, Phys. Rev. Lett. **127**, 113201 (2021).

[11] C. K. Ong, G. M. Huang, T. J. Tarn, and J. W. Clark, Invertibility of quantum-mechanical control systems, Math. Syst. Theory **17**, 335 (1984).

[12] J. W. Clark, C. K. Ong, T. J. Tarn, and G. M. Huang, Quantum nondemolition filters, Math. Syst. Theory **18**, 33 (1985).

[13] A. Jha, V. Beltrani, C. Rosenthal, and H. Rabitz, Multiple Solutions in the Tracking Control of Quantum Systems, J. Phys. Chem. A **113**, 7667 (2009).

[14] G. McCaul, A. F. King, and D. I. Bondar, Non-uniqueness of non-linear optical response, arXiv:2110.06189.

[15] R. Y. Chiao, E. Garmire, and C. H. Townes, Self-Trapping of Optical Beams, Phys. Rev. Lett. **13**, 479 (1964).

[16] M. Kroner, A. O. Govorov, S. Remi, B. Biedermann, S. Seidl, A. Badolato, P. M. Petroff, W. Zhang, R. Barbour, B. D. Gerardot, R. J. Warburton, and K. Karrai, The nonlinear fano effect, Nature (London) **451**, 311 (2008).

[17] Y.-R. Shen, *The Principles of Nonlinear Optics* (John Wiley & Sons, New York, 1984).

[18] C. B. de Araújo, A. S. L. Gomes, and G. Boudebs, Techniques for nonlinear optical characterization of materials: A review, Rep. Prog. Phys. **79**, 036401 (2016).

[19] R. W. Boyd, *Nonlinear Optics*, 3rd ed. (Academic, Amsterdam/Boston, 2008).

[20] J. Itatani, J. Levesque, D. Zeidler, H. Niikura, H. Pépin, J. C. Kieffer, P. B. Corkum, and D. M. Villeneuve, Tomographic imaging of molecular orbitals, Nature (London) **432**, 867 (2004).

[21] N. Hay, R. Velotta, M. Lein, R. de Nalda, E. Heesel, M. Castillejo, and J. P. Marangos, High-order harmonic generation in laser-aligned molecules, Phys. Rev. A **65**, 053805 (2002).

[22] M. Lein, N. Hay, R. Velotta, J. P. Marangos, and P. L. Knight, Interference effects in high-order harmonic generation with molecules, Phys. Rev. A **66**, 023805 (2002).

[23] M. Lein, P. P. Corso, J. P. Marangos, and P. L. Knight, Orientation dependence of high-order harmonic generation in molecules, Phys. Rev. A **67**, 023819 (2003).

[24] G. L. Kamta and A. D. Bandrauk, High-order harmonic generation from two-center molecules: Time-profile analysis of nuclear contributions, Phys. Rev. A **70**, 011404(R) (2004).

[25] G. L. Kamta and A. D. Bandrauk, Three-dimensional time-profile analysis of high-order harmonic generation in molecules: Nuclear interferences in h_2^+, Phys. Rev. A **71**, 053407 (2005).

[26] M. Eidi, M. Vafaee, H. Koochaki Kelardeh, and A. Landsman, High-order harmonic generation by static coherent states method in single-electron atomic and molecular systems, J. Comput. Chem. **42**, 1312 (2021).

[27] D. von der Linde, T. Engers, G. Jenke, P. Agostini, G. Grillon, E. Nibbering, A. Mysyrowicz, and A. Antonetti, Generation of high-order harmonics from solid surfaces by intense femtosecond laser pulses, Phys. Rev. A **52**, R25(R) (1995).

[28] B. Dromey, M. Zepf, A. Gopal, K. Lancaster, M. S. Wei, K. Krushelnick, M. Tatarakis, N. Vakakis, S. Moustaizis, R. Kodama, M. Tampo, C. Stoeckl, R. Clarke, H. Habara, D.

Neely, S. Karsch, and P. Norreys, High harmonic generation in the relativistic limit, Nat. Phys. **2**, 456 (2006).

[29] G. Vampa, C. R. McDonald, G. Orlando, D. D. Klug, P. B. Corkum, and T. Brabec, Theoretical Analysis of High-Harmonic Generation in Solids, Phys. Rev. Lett. **113**, 073901 (2014).

[30] S. Y. Kruchinin, F. Krausz, and V. S. Yakovlev, Colloquium: Strong-field phenomena in periodic systems, Rev. Mod. Phys. **90**, 021002 (2018).

[31] L. Ortmann and A. S. Landsman, *High-Harmonic Generation in Solids* (Academic, Cambridge, MA, 2021), Chap. 2, pp. 103–156.

[32] S. Ghimire, A. D. DiChiara, E. Sistrunk, P. Agostini, L. F. DiMauro, and D. A. Reis, Observation of high-order harmonic generation in a bulk crystal, Nat. Phys. **7**, 138 (2011).

[33] G. Vampa, T. J. Hammond, N. Thiré, B. E. Schmidt, F. Légaré, C. R. McDonald, T. Brabec, and P. B. Corkum, Linking high harmonics from gases and solids, Nature (London) **522**, 462 (2015).

[34] G. Ndabashimiye, S. Ghimire, M. Wu, D. A. Browne, K. J. Schafer, M. B. Gaarde, and D. A. Reis, Solid-state harmonics beyond the atomic limit, Nature (London) **534**, 520 (2016).

[35] T. T. Luu, M. Garg, S. Y. Kruchinin, A. Moulet, M. T. Hassan, and E. Goulielmakis, Extreme ultraviolet high-harmonic spectroscopy of solids, Nature (London) **521**, 498 (2015).

[36] M. Hohenleutner, F. Langer, O. Schubert, M. Knorr, U. Huttner, S. W. Koch, M. Kira, and R. Huber, Real-time observation of interfering crystal electrons in high-harmonic generation, Nature (London) **523**, 572 (2015).

[37] F. Langer, M. Hohenleutner, C. P. Schmid, C. Poellmann, P. Nagler, T. Korn, C. Schüller, M. S. Sherwin, U. Huttner, J. T. Steiner, S. W. Koch, M. Kira, and R. Huber, Lightwave-driven quasiparticle collisions on a subcycle timescale, Nature (London) **533**, 225 (2016).

[38] N. Yoshikawa, T. Tamaya, and K. Tanaka, High-harmonic generation in graphene enhanced by elliptically polarized light excitation, Science **356**, 736 (2017).

[39] H. Liu, Y. Li, Y. S. You, S. Ghimire, T. F. Heinz, and D. A. Reis, High-harmonic generation from an atomically thin semiconductor, Nat. Phys. **13**, 262 (2017).

[40] Y. S. You, D. Reis, and S. Ghimire, Anisotropic high-harmonic generation in bulkÂ crystals, Nat. Phys. **13**, 345 (2017).

[41] U. Huttner, M. Kira, and S. W. Koch, Ultrahigh off-resonant field effects in semiconductors, Laser Photonics Rev. **11**, 1700049 (2017).

[42] M. F. Ciappina, J. A. Pérez-Hernández, A. S. Landsman, W. A. Okell, S. Zherebtsov, B. Förg, J. Schötz, L. Seiffert, T. Fennel, T. Shaaran, T. Zimmermann, A. Chacón, R. Guichard, A. Zaïr, J. W. G. Tisch, J. P. Marangos, T. Witting, A. Braun, S. A. Maier, L. Roso *et al.*, Attosecond physics at the nanoscale, Rep. Prog. Phys. **80**, 054401 (2017).

[43] M. Drescher, M. Hentschel, R. Kienberger, G. Tempea, C. Spielmann, G. A. Reider, P. B. Corkum, and F. Krausz, X-ray pulses approaching the attosecond frontier, Science **291**, 1923 (2001).

[44] P. M. Paul, E. S. Toma, P. Breger, G. Mullot, F. Augé, P. Balcou, H. G. Muller, and P. Agostini, Observation of a train of attosecond pulses from high harmonic generation, Science **292**, 1689 (2001).

[45] M. Hentschel, R. Kienberger, C. Spielmann, G. A. Reider, N. Milosevic, T. Brabec, P. Corkum, U. Heinzmann, M. Drescher, and F. Krausz, Attosecond metrology, Nature (London) **414**, 509 (2001).

[46] F. Krausz and M. Ivanov, Attosecond physics, Rev. Mod. Phys. **81**, 163 (2009).

[47] A. S. Landsman and U. Keller, Attosecond science and the tunnelling time problem, Phys. Rep. **547**, 1 (2015), attosecond science and the tunneling time problem.

[48] A. B. Magann, G. McCaul, H. A. Rabitz, and D. I. Bondar, Sequential optical response suppression for chemical mixture characterization, Quantum **6**, 626 (2022).

[49] F. Krausz, From femtochemistry to attophysics, Phys. World **14**, 41 (2001).

[50] R. Cireasa, A. E. Boguslavskiy, B. Pons, M. C. H. Wong, D. Descamps, S. Petit, H. Ruf, N. Thiré, A. Ferré, J. Suarez, J. Higuet, B. E. Schmidt, A. F. Alharbi, F. Légaré, V. Blanchet, B. Fabre, S. Patchkovskii, O. Smirnova, Y. Mairesse, and V. R. Bhardwaj, Probing molecular chirality on a sub-femtosecond timescale, Nat. Phys. **11**, 654 (2015).

[51] O. Neufeld, D. Ayuso, P. Decleva, M. Y. Ivanov, O. Smirnova, and O. Cohen, Ultrasensitive Chiral Spectroscopy by Dynamical Symmetry Breaking in High Harmonic Generation, Phys. Rev. X **9**, 031002 (2019).

[52] Á. Jiménez-Galán, R. E. Silva, O. Smirnova, and M. Ivanov, Sub-cycle valleytronics: Control of valley polarization using few-cycle linearly polarized pulses, Optica **8**, 277 (2021).

[53] J. Lee, K.-H. Jin, and H. W. Yeom, Distinguishing a Mott Insulator from a Trivial Insulator with Atomic Adsorbates, Phys. Rev. Lett. **126**, 196405 (2021).

[54] M. Chergui and A. H. Zewail, Electron and x-ray methods of ultrafast structural dynamics: Advances and applications, ChemPhysChem **10**, 28 (2009).

[55] M. Lein, N. Hay, R. Velotta, J. P. Marangos, and P. L. Knight, Role of the Intramolecular Phase in High-Harmonic Generation, Phys. Rev. Lett. **88**, 183903 (2002).

[56] C. Shao, H. Lu, X. Zhang, C. Yu, T. Tohyama, and R. Lu, High-Harmonic Generation Approaching the Quantum Critical Point of Strongly Correlated Systems, Phys. Rev. Lett. **128**, 047401 (2022).

[57] M. Garg, A. Martin-Jimenez, M. Pisarra, Y. Luo, F. Martín, and K. Kern, Real-space subfemtosecond imaging of quantum electronic coherences in molecules, Nat. Photonics **16**, 196 (2021).

[58] S. H. Simon, *The Oxford Solid State Basics* (Oxford University Press, Oxford, 2013).

[59] F. Essler, H. Frahm, F. Gohmann, A. Klumper, and V. Korepin, *The One-Dimensional Hubbard Model* (Cambridge University Press, Cambridge, UK, 2005).

[60] Y. Murakami, M. Eckstein, and P. Werner, High-Harmonic Generation in Mott Insulators, Phys. Rev. Lett. **121**, 057405 (2018).

[61] S. Imai, A. Ono, and S. Ishihara, High Harmonic Generation in a Correlated Electron System, Phys. Rev. Lett. **124**, 157404 (2020).

[62] R. E. F. Silva, I. V. Blinov, A. N. Rubtsov, O. Smirnova, and M. Ivanov, High-harmonic spectroscopy of ultrafast many-body

dynamics in strongly correlated systems, Nat. Photonics **12**, 266 (2018).

[63] N. Ashcroft and N. Mermin, *Solid State Physics* (Saunders College, Philadelphia, 1976).

[64] T. Oka, Nonlinear doublon production in a mott insulator: Landau-dykhne method applied to an integrable model, Phys. Rev. B **86**, 075148 (2012).

[65] L. Keldysh, Ionization in the field of a strong electromagnetic wave, Sov. Phys. JETP **20**, 1307 (1965).

[66] C. A. Stafford, A. J. Millis, and B. S. Shastry, Finite-size effects on the optical conductivity of a half-filled hubbard ring, Phys. Rev. B **43**, 13660 (1991).

[67] J. L. Krause, K. J. Schafer, and K. C. Kulander, High-Order Harmonic Generation from Atoms and Ions in the High Intensity Regime, Phys. Rev. Lett. **68**, 3535 (1992).

[68] T. Oka and S. Kitamura, Floquet engineering of quantum materials, Annu. Rev. Condens. Matter Phys. **10**, 387 (2019).

[69] S. Blanes, F. Casas, J. Oteo, and J. Ros, The magnus expansion and some of its applications, Phys. Rep. **470**, 151238 (2009).

[70] DLMF, NIST Digital Library of Mathematical Functions, edited by f. W. J. Olver, A. B. Olde Daalhuis, D. W. Lozier, B. I. Schneider, R. F. Boisvert, C. W. Clark, B. R. Miller, B. V. Saunders, H. S. Cohl, and M. A. McClain, http://dlmf.nist.gov/, Release 1.1.3 of 2021-09-15.

[71] P. Weinberg and M. Bukov, QUSPIN: A Python Package for Dynamics and Exact Diagonalisation of Quantum Many Body Systems. Part II: bosons, fermions and higher spins, SciPost Phys. **7**, 020 (2019).

[72] L. Tolstoy, *Anna Karenina: A Novel in Eight Parts* (Penguin Classics, London, 2013).

[73] V. Heine and L. F. Mattheiss, Metal-insulator transition in transition metal oxides, J. Phys. C **4**, L191 (1971).

[74] T. D. Dorney, R. G. Baraniuk, and D. M. Mittleman, Material parameter estimation with terahertz time-domain spectroscopy, J. Opt. Soc. Am. A **18**, 1562 (2001).

[75] J. Neu and C. A. Schmuttenmaer, Tutorial: An introduction to terahertz time domain spectroscopy (thz-tds), J. Appl. Phys. **124**, 231101 (2018).